Procedia Manufacturing

Volume 5, 2016, Pages 815–827

44th Proceedings of the North American Manufacturing Research Institution of SME http://www.sme.org/namrc

Rake Face Temperature when Machining with Coated Cutting Tools

Jean Carlos Garcia-Gonzalez, Wilfredo Moscoso-Kingsley, Viswanathan Madhavan*

Wichita State University, Wichita, U.S.A.

Abstract

Infrared thermography through transparent cutting tools has been used to measure the chip-tool interface temperature. It is of interest to extend this technique to study changes in interface temperature when tool coatings are used. An initial attempt is made here to measure the chip-tool interface temperature distribution when cutting Ti6Al4V with a TiN coated YAG tool. The TiN coating thickness is kept low at about 100 nm to minimize the temperature difference between the front (chip-TiN interface) and the back (TiN-YAG interface) faces of the coating. The transparency of the YAG tool allows near infrared radiation emitted by the back face of the TiN coating to be imaged. A novel method is used to measure the emissivity of the TiN/YAG interface. Using this method, and the available blackbody calibration of the temperature vs. intensity response of the imaging system, the images are converted into temperature maps. The performance of the coated tool is also evaluated in terms of machining force and tool wear characteristics. Coatings that remain intact during the experiments will reduce ambiguity in interpretation of the results.

Keywords: Machining, tool coatings, tool temperature, thermography.

1 Introduction

This paper introduces an extension of infrared thermography through transparent cutting tools for evaluation of the performance of machining tool coatings in terms of the temperature distribution that develops at the tool rake face. The technique consists of the application of an industrially relevant coating on an optically transparent material having the shape of a cutting tool. The temperature at the interface between coating and tool is then measured by *in situ* imaging of visible and near infrared radiation emitted. The coating is made sufficiently thick to withstand the cutting, yet thin enough that the temperature at the chip-coating interface is essentially the same as the temperature directly measured at the coating underside. Unlike other methods of tool temperature measurement that

*Corresponding Author. Email: vis.madhavan@wichita.edu.

Selection and peer-review under responsibility of the Scientific Programme Committee of NAMRI/SME

doi:10.1016/j.promfg.2016.08.066

measure point-wise or average temperatures close to the interface, this technique provides the actual chip-tool interface temperature distribution that controls coating wear. In principle, the measurements can be performed for any industrial-grade tool coating or material. This technique is demonstrated here using titanium nitride (TiN) as coating material and yttrium aluminum garnet (YAG) as cutting tool body. For the demonstration, the workpiece material was annealed titanium alloy Ti6Al4V.

As the chip slides across the coated rake face, a thermographic system is used to image the radiation emitted by the coating underside (the side in contact with the tool), as shown in Figure 1. Following calibration with a blackbody, the radiation is then converted to temperature. For the conversion, the emissivity of the coating material must be known. The novel approach makes use of the reflection of the tool rake face on the tool flank face, which is also coated, to determine the coating emissivity *in situ*. The coating is sufficiently thin that the temperature difference across its thickness is negligible. Thus, the temperature at the chip-coating interface is virtually directly measured. This statement was justified using a simple one-dimensional heat transfer model. To ensure accuracy for the target temperature of about 1250 K, near infrared (visible) thermography was actually used, as explained by Lane et al., and Menon and Madhavan (Lane, Whitenton, Madhavan, & Donmez, 2013; Menon & Madhavan, 2014).

Attempts to measure temperature at the actual point where heat is generated in machining date back to the works of Shore (Shore, 1925) and Herbert (Herbert, 1926), who introduced the tool-work thermocouple technique. Among different methods that have been implemented since then stand out thermometry by the use of embedded thermocouples (Kitagawa, Kubo, & Maekawa, 1997), metallographic analysis (Wright & Trent, 1974; Smart & Trent, 1975) and radiometry, which in turn can be subdivided into pyrometry and infrared and near infrared thermography (Boothroyd, 1963; Jaspers, Dautzenberg, & Taminiau, 1998; Kus, Isik, Cemal Cakir, Coskun, & Özdemir, 2015; Lane, Whitenton, Madhavan, & Donmez, 2013; Menon & Madhavan, 2014). The tool-work thermocouple technique is based on the existence of a thermoelectric effect at the chip-tool interface, provided that the workpiece and the tool materials are dissimilar. It can only measure the mean temperature at the chip-tool interface. While it is possible to place many thermocouples very close to the chip-tool interface (embedded thermocouples) to determine temperature distribution at this interface (Komanduri & Hou, 2001), the installation of these thermocouples can be cost intensive and extremely tedious. More importantly, multiple holes have to be drilled, which alters the heat conduction through the tool and reduces its strength. Metallographic techniques infer the chip-tool interface temperature from microstructural or hardness changes in the chip material directly in contact with the tool. Even though this method is capable of measuring temperature within ±25 K in the range of 900 K to 1150 K (Wright & Trent, 1974), it is only applicable to tool materials whose microstructural change is very sensible to temperature, such as high speed steels.

In thermography, the radiation emitted by different points of a hot source in the infrared or near infrared portion of the spectrum can be converted into source temperature using a power law in the form (Menon & Madhavan, 2014; Menon, 2013):

$$T = a\left(\frac{S}{\varepsilon\tau}\right)^{b} \tag{1}$$

where T is the temperature of a particular point on the object (in Kelvin, K), S is a measure of the radiation intensity reaching the camera pixel where the object point is imaged, also known as the "counts" and expressed in arbitrary units, ε is the emissivity of the object's surface (dimensionless), and τ is the camera exposure time (in milliseconds, ms). The constants in Equation 1 are obtained after calibration with a blackbody placed directly on top of the tool rake face. The calibration procedure has been well described by Menon and Madhavan (Menon & Madhavan, 2014; Menon, 2013). If the radiation is measured with a high speed camera, thermography can return the temperature distribution of the source surface with high spatial and temporal resolution. This technique has been used to investigate the temperature distribution of the cutting tool (Miller, Mulholland, & Anderson, 2003; Narayanan, Krishnamurthy, Chandrasekar, Farris, & Madhavan, 2001), the workpiece (Boothroyd,

1963), the chip side faces (Sutter & Ranc, 2007), the top of the chip (Jaspers, Dautzenberg, & Taminiau, 1998), and the chip-tool interface (Davies, Yoon, Schmitz, Burns, & Kennedy, 2003). The use of thermography to determine the chip-tool interface temperature distribution requires optical access to the tool rake face. This has been accomplished through the use of tools that are transparent in the infrared and the near infrared.

Müller-Hummel and Lahres (Müller-Hummel & Lahres, 1994; Müller-Hummel & Lahres, 1995) and Müller-Hummel et al. (Müller-Hummel, Lahres, Mehlhose, & Lang, 1997) used tools furbished with a 5-µm thick layer of chemical vapor deposition (CVD) diamond, which had a 500-µm thick window on a portion of the tool rake face. The window was sufficiently strong to withstand the cutting forces. A mirror underneath the window projected an image of the radiation emitted by the chip surface in contact with the window during the three-dimensional (3D) cutting of titanium and aluminum alloys. The camera was sensible to infrared radiation. The aim of the work was to find a correlation between chip-tool interface temperature and tool wear. Temperatures as high as 2000 K were reported for Ti6Al4V at machining velocities of about 2.5 m/s and feeds of about 300 µm/rev; and for AlZnMgCu1.5, at 21.7 m/s machining velocity and 400 µm/rev feed, temperatures were as high as 800 K. According to work reported by Davies et al. (Davies, Yoon, Schmitz, Burns, & Kennedy, 2003), for the temperature range produced at the machining velocity and feed that were applied above, the uncertainty in emissivity in the infrared leads to a relatively large error in temperature estimate. That is, about +/- 50 K (Davies, Yoon, Schmitz, Burns, & Kennedy, 2003). In addition to the high uncertainty inherent to infrared thermography, the CVD diamond window allowed only partial observation of the temperature field at the tool rake face. More accurate methods for observation of the full field temperature distribution at the tool rake face are desirable.

Narayanan et al. (Narayanan, Krishnamurthy, Chandrasekar, Farris, & Madhavan, 2001), measured the temperature distribution of the chip-tool interface when cutting brass in a two-dimensional (2D) orthogonal arrangement using optically transparent sapphire tools. These tools were optically transparent in both the infrared and near infrared bands, and thus allowed the use of multi-wavelength high speed infrared pyrometry. These sapphire tools were much simpler than the CVD tools of Müller-Hummel and Lahres, and the multi-wavelength technique compensated for unknown emissivity values. The results showed that the highest temperature occurred in the zone of metal deposits some distance away from the cutting edge and on sides of the chip-tool contact. Temperatures as high as ~700 K were reported at machining velocities of about 1.5 m/s and feeds of about 50 µm/rev. While sapphire is sufficiently transparent and inexpensive to allow full size tools to be made, due to its significant decrease in hardness above 1000 K, cutting tools made out of this material are not suitable for the cutting of industrially-relevant, hard materials.

Menon and Madhavan (Menon & Madhavan, 2014) measured the temperature distribution of the chip-tool interface when cutting Ti6Al4V in a two-dimensional (2D) orthogonal arrangement using optically transparent yttrium aluminum garnet (YAG) tools. Near infrared thermography was implemented as a technique to reduce temperature uncertainty. For temperatures of about 1250 K, Menon and Madhavan reported uncertainty in temperature of less than 10 K. The YAG crystals were also sufficiently transparent and inexpensive to allow full size tools to be made.

While the use of transparent tooling has enabled the observation of the rake face temperature distribution, it has also left some fundamental questions unanswered. Will the use of transparent tooling in lieu of the typical cutting tool materials utilized in industry introduce an inherently different chip-tool contact condition, and rake face temperature? If an industrial cutting tool material is used, how different would the temperature readings be? As a unique contribution of the present work, and to address these questions, the use of optically transparent tools coated with a nanometric layer of an industrial anti-friction/wear resistant material is outlined. An attempt to produce such coated tools, and perform measurements of the chip-tool temperature is described in this paper.

2 Experimental Configuration

The machining experiments for the observation of tool temperature were carried out using a very rigid and high speed custom-built lathe. The setup was arranged in a way that allowed the cutting tool to be held stationary while the rotating workpiece was fed into the tool, as shown in Figure 1. The loop stiffness of the lathe was in the order of 100 N/µm. The spindle was capable of rotating at up to 10,000 rpm. The tool holder had a small pocket where a glass front-surface mirror was mounted (inset in Figure 1). The mirror directed the radiation emitted by the surface of the coating in contact with the tool rake face towards the camera, as shown in Figure 1. The tool holder was mounted on a Kistler 9367B tri-axial dynamometer that measured the cutting and thrust force.

The workpieces were prepared from solid rods of annealed Ti6Al4V. The rods were all turned to 25.4 mm diameter (OD). Then, drilling and boring was completed to form tubes. The tubes had wall thickness = 1.07 mm. The tubes were held by a collet on the lathe that allowed a firm installation with minimal runout. Since the rotating workpiece was a narrow wall tube, the adopted configuration approximated 2-D orthogonal cutting. For each of the cuts, the total cutting length was 0.48 m.

A YAG cube was coated with titanium nitride (TiN) using a Denton Discovery-550 Vacuum Sputtering System available at the Center for Nanoscale Science and Technology (CNST) of the National Institute of Standards and Technology (NIST). A TiN target was used in a pure argon atmosphere (flow rate of 50 sccm and pressure of 0.47 Pa) at 25 °C. A DC gun was used at 300 W (with a RF bias of 100 W) and the target was cleaned by pre-sputtering for 120 s prior to the deposition time of 350 s. This resulted in a TiN coating on the top face of the YAG cube that was 100 nm thick, and there was also significant deposition on all four adjoining faces. This cube was used as the cutting tool with the bottom uncoated face being the face through which the observation was carried out, and each of the four edges of the top face were used as cutting edges in successive experiments. The machining velocity (V) was 1 m/s, and the feed (f) was 50 µm/rev. The tool rake and relief angles were -5° and 5°, respectively. The tool cutting edge was nominally sharp (about 2.5-µm edge radius).

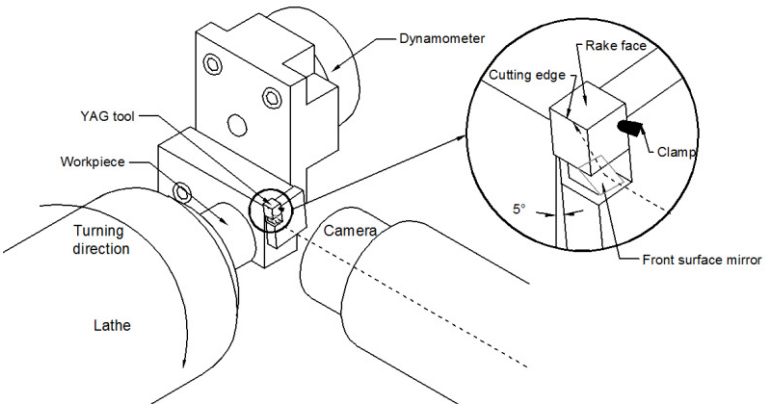

Figure 1: Schematic of the experimental setup.

The YAG cubes, supplied by Red Optronics, were 6-mm cubes having 12 potentially usable cutting edges. To increase the toughness of the YAG cubes, they were subject to an annealing treatment in air in a Sentro Tech Corp. STT-1600-2.75-12 high temperature tube furnace. The YAG cubes were heated at a rate of 4 °C per minute, held at 1600 °C for 10 hours and then cooled back to ambient temperature at a rate of 4 °C per minute. Then, the TiN coating was deposited at the CNST

(NIST). Care was taken to observe under the microscope (a MicroXAM optical profilometer) the edge condition of these tools after annealing and prior to cutting. The same profilometer was used to observe the tool condition after cutting.

The radiation was imaged by a LaVision Imager Intense cooled low noise camera that was mounted on a Leica MZ16 stereomicroscope. A 1x plan apochromatic objective (numerical aperture = NA = 0.14) and a 1.5x coupler were used along with an 8x optical zoom to achieve an effective magnification of 12x on the 1376 x 1024 charge-coupled device (CCD) array in the camera. Therefore, each 6.45-µm square pixel was equivalent to approximately a 0.56-µm square region of the tool surface, and the total field of view was 770 µm x 570 µm. Figure 2A shows the radiation captured by the camera. The figure shows the orientation of the cutting edge in the image. A direct image of the tool rake face is projected on the CCD array to the right of the cutting edge. The rake face also reflects from the flank face. This reflected image reaches the CCD array, and projects to the left of the cutting edge. Figure 2B shows the conversion to temperature vs. distance from the cutting edge superimposed on a micrograph of the tool rake face. To convert radiation intensity to temperature, Equation 1 was applied pixel-by-pixel. The constants *a* and *b* in Equation 1 were 1036.65 and 0.0647, respectively (Menon & Madhavan, 2014; Menon, 2013).

The camera had a 12-bit dynamic range (4095 counts), with readout noise less than 2.5 counts, dark noise less than 1 count, nonlinearity less than 1% and non-uniformity less than 0.6%. The exposure time was selected on the basis of intensity reaching the CCD array. The selection was made to avoid both low counts too close to noise level and high counts too close to saturation. The laboratory was darkened to start the experiments. Background images at room temperature were taken prior to each cutting experiment, which usually resulted in intensity of about 40 counts. The background images were averaged and subtracted pixel-by-pixel from the *in situ* images.

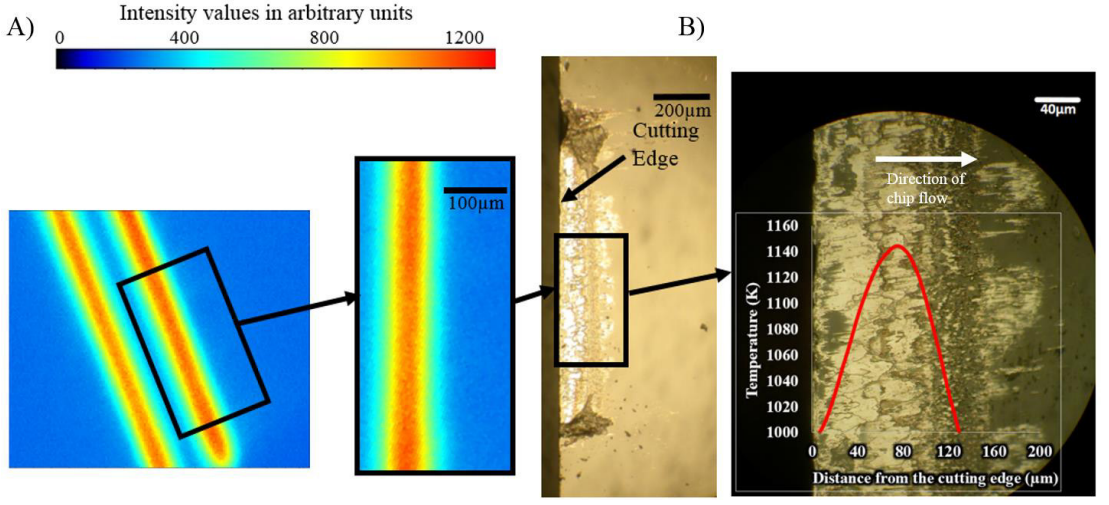

Figure 2: A) Actual image recorded by the camera system. B) Conversion to temperature vs. distance from the cutting edge superimposed on a micrograph of the tool rake face.

3 Experimental Results

Prior to interpretation of radiation measurements, the emissivity of the target surface must be determined. For the uncoated tool, the target surface is the chip underside in direct contact with the

tool rake face (the transparent YAG substrate). The emissivity of the Ti6Al4V chip material was taken as 0.5, as per work reported by Menon and Madhavan (Menon & Madhavan, 2014; Menon, 2013). For the coated tool, the target surface is the coating underside in direct contact with the tool rake face (the transparent YAG substrate). The emissivity of the TiN coating was measured *in situ,* by taking advantage of the unique configuration offered by the coated YAG cube, which had the tool rake and flank faces coated. Figure 3 shows the intensity profiles of both the image coming directly from the coated rake face, and the image reflected on the coated flank face. Note that the intensity of the direct image is significantly larger than that of the reflected image. The reflected image is also narrower, possibly due to lensing effects from a flank face that is not perfectly planar. The reflected image was first spread to match the width of the direct image (Figure 3), and then, for pixels equidistant from the tool cutting edge, the intensity of the reflected image was divided by the intensity of the direct image. The result is shown in Figure 3. Note that this ratio, which is a measure of the reflectivity of TiN is essentially constant for a portion of the space between the cutting edge and the point of departure of the chip from the tool. The mean reflectivity over the region where the ratio is essentially constant is 0.75. This implies that the emissivity of TiN is about 0.25.

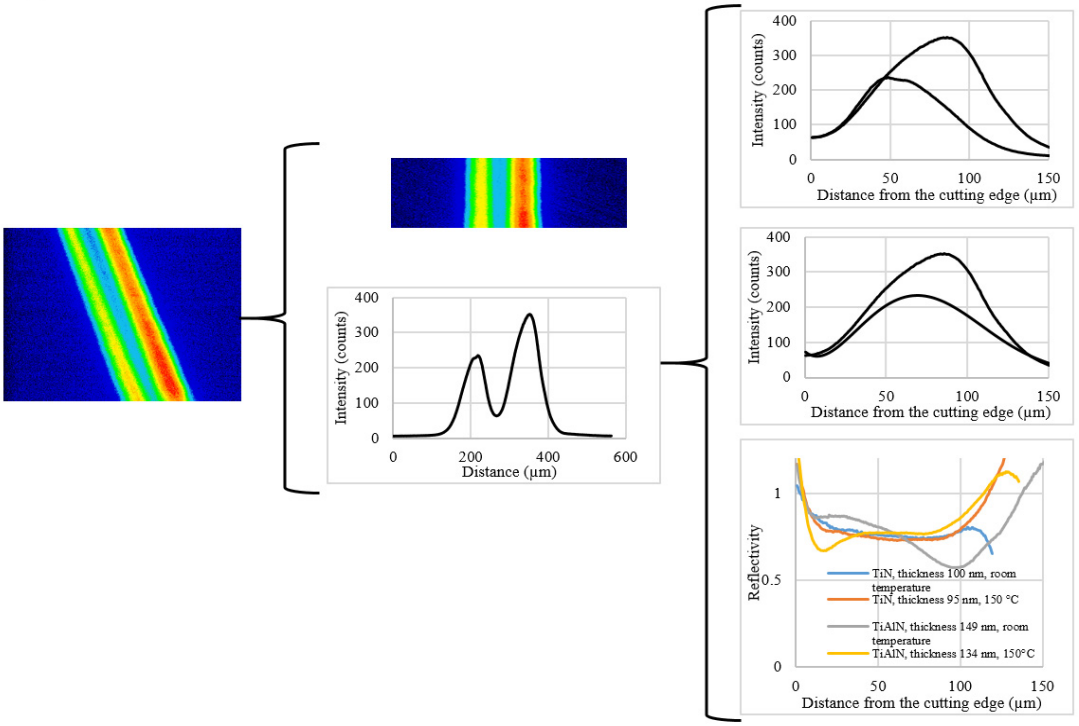

Figure 3: Image manipulation used to estimate the emissivity of TiN *in situ*.

The radiation intensity and temperature distributions at the chip-tool contact, when using both the coated and the uncoated tools are shown in Figure 4A and 4B, respectively. The cutting and thrust forces for the coated and the uncoated tools are shown in Figure 5. Table 1 shows summary statistics obtained from the force data, along with total power and friction power computed from the force measurements at the set machining velocity. For friction power, the chip thickness was measured using a micrometer.

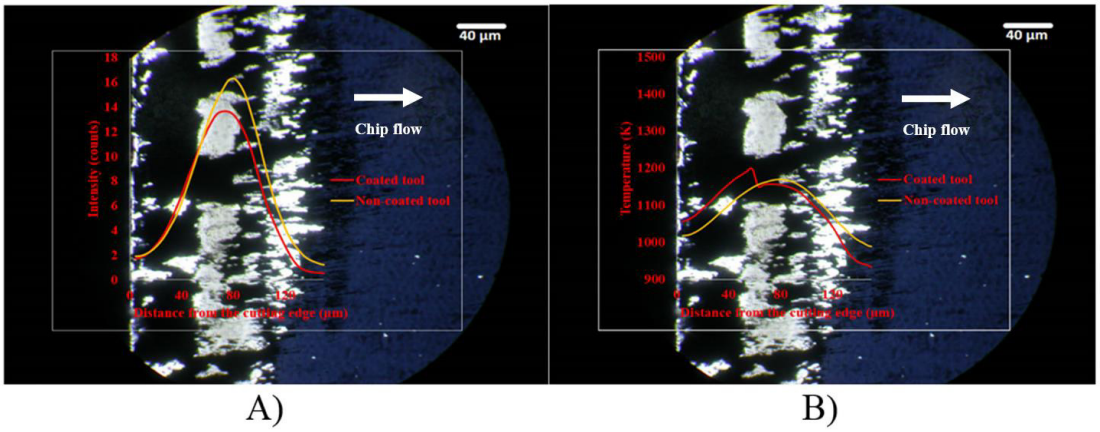

Figure 4: Image of the rake face of the used cutting tool illuminated from the bottom showing dark regions where the coating is intact and light regions where the coating is removed. Superimposed on this image is A) intensity counts (in arbitrary units) as a function of distance from the cutting edge. The red trace is for the coated tool. The yellow trace is for the control non-coated tool, and B) temperatures calculated from the intensity profiles. The red trace is for the coated tool. The yellow trace is for the non-coated tool. $V = 1$ m/s, $f = 50$ µm/rev.

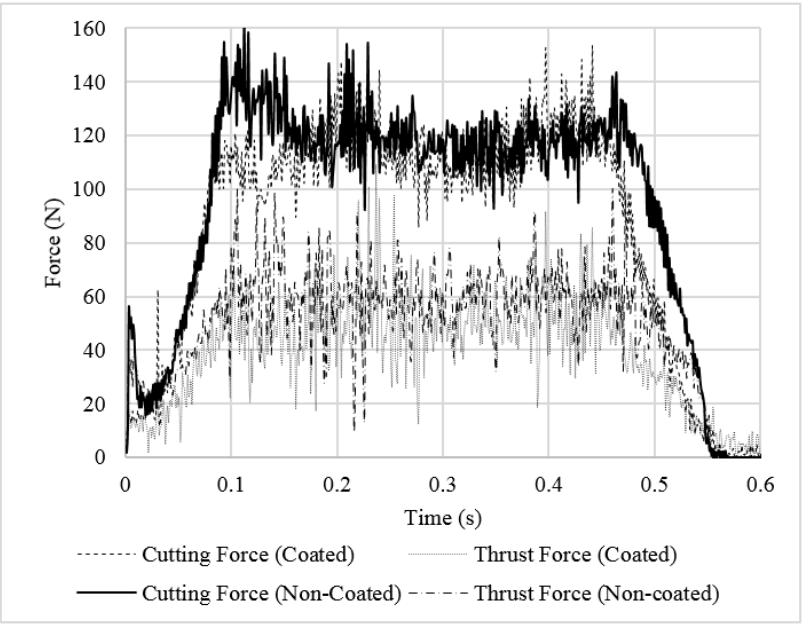

Figure 5: Normal and friction forces acting on the tool rake face for both the coated and the control non-coated tools. The decrease in forces after application of the TiN coating is consistent with a coating that has at least partially survived the cutting, as suggested in Figure 6. $V = 1$ m/s, $f = 50$ µm/rev.

	TiN-YAG Tool	Uncoated Tool
Cutting Force (N)	113+/-11	120.88+/-12
Thrust Force (N)	49.99+/-14	60.77+/-13
Normal Force (N)	117	126
Friction Force (N	40	50
Total Power (W)	113	121
Friction Power (W)	25*	35**

*Chip thickness ratio = 0.6. **Chip thickness ratio = 0.7. V = 1 m/s, f = 50 µm/rev.

Table 1: Summary statistics from Figure 5.

During the cutting experiment, the TiN coating was removed from the tool rake face in places, as observed in the micrographs of Figure 6. Figure 6A shows the top side of the coating while it is illuminated from the bottom side with a small lamp. The "pale blue" regions correspond to light shining through the damaged coating. Note that there is a color difference between the rough area adjacent to the cutting edge, and the smooth area away from the cutting edge. The color difference suggests that there may be Ti6Al4V deposits on the tool, either on the TiN or the YAG. Figure 6B shows the coating bottom side. This view shows that there is a region about 57 µm wide that mostly has the same color as that away from the cutting edge. This suggests that the Ti6Al4V deposits near the cutting edge lie on top of a layer of TiN coating that might be thinned out, but is continuous for the most part. Immediately after this lightly damaged region, there is a ~50-µm wide region that is heavily damaged. Note that these observations are consistent with the wear profile in Figure 7, and that coating damage occurs where the temperature is highest. Moreover, the coating damage occurs were crater wear is usually observed when cutting Ti6Al4V with the uncoated tools. When uncoated YAG tools are used at the same cutting conditions (V = 1 m/s and f = 50 µm/rev), crater depth is less than 0.5 µm.

The coating remained essentially intact near the cutting edge, and peeled off the tool rake face away from the cutting edge. For temperature calculations (Figure 4B), the surface emissivity in the vicinity of the cutting edge was taken as that of the TiN coating, and the surface emissivity away from the cutting edge was taken as that of the Ti6Al4V chip. However, the use of these emissivity values produces a discontinuity in the temperature profile (Figure 4B), which raises questions about the accuracy of the temperature estimate.

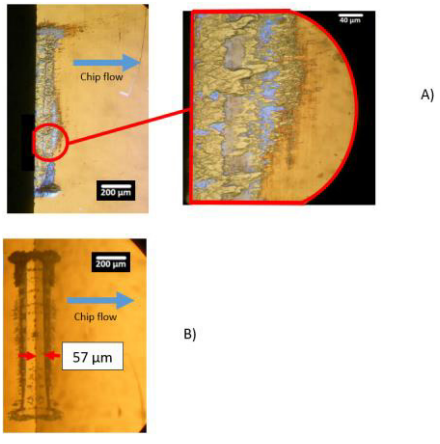

Figure 6: Rake face views. A) Coating top (free) side while it is illuminated from the bottom side with a small lamp. B) Coating bottom (YAG) side.

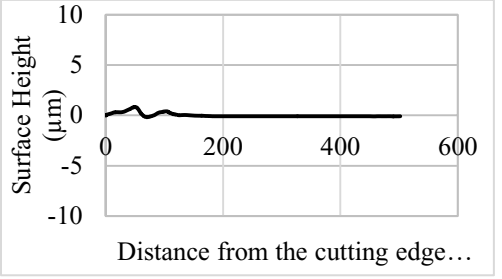

Figure 7: Surface profile of cutting tool as distance from the cutting edge (0 µm = cutting edge position). Profile heights above zero are consistent with the Ti6Al4V deposits in Figure 6.

4 Temperature Difference through the Coating Thickness

If the chip formation process is at thermal steady state, then conduction through the coating would be represented by the following equation (Incropera, Dewitt, Bergman, & Lavine):

$$q'' = \frac{k}{L}(T_C - T_U), \tag{2}$$

where q'' is the heat flux (in W/m^2) crossing the chip-coating interface area, L is the coating thickness (in m), T_c is the temperature at the chip-coating interface (in K), T_u is the temperature at the coating-tool interface (in K), and k is the thermal conductivity of the coating. For the TiN coating utilized here, k = 19.2 W/m-K (Pierson, 1996). From Equation 2, the temperature gradient across the coating thickness would be:

$$\frac{T_C - T_U}{L} = \frac{q''}{k} = \frac{q''}{19.2\,{}^{W}/_{m\text{-}K}}. \tag{3}$$

Assuming that all the heat produced by friction at the chip-tool interface flows into the tool (which is highly conservative since only a small fraction, represented by the heat partition coefficient, flows into the tool), its magnitude would be equal to the friction power (P_F, in W) at the chip-tool interface divided by the chip-tool interface area (A, in m^2). From force measurements, as shown in Table 1, the friction power for V = 1 m/s and f = 50 µm/rev would be approximately 25 W. The chip-tool interface area is width of cut x chip-tool contact length. The width of cut is 1.07 mm, and the chip-tool contact length is approximately 1.5 x feed = 75 µm. Thus,

$$q'' = \frac{P_F}{A} = 3.3x10^8\,\frac{W}{m^2}, \tag{4}$$

and

$$\frac{T_C - T_U}{L} = \frac{(3.3x10^8 \mathrm{W/m^2})}{19.2\mathrm{W/m\text{-}K}} = 17.4\,\frac{\mathrm{K}}{\mu\mathrm{m}}. \tag{5}$$

For the 100-nm coating utilized in the experiments, the temperature drop across the coating would be 1.74 K, which is within the uncertainty of the thermographic camera. This implies that measurement of the coating-tool interface temperature is equivalent to measurement of the chip-coating interface temperature. This also implies that the temperature measured at the chip-tool interface when using the uncoated tool is directly comparable to the temperature measured at the coating-tool interface when using the TiN-YAG tool. As long as machining parameters (machining velocity, feed, etc.) remain the same, and the comparisons are made after sufficient time into the cut, comparing the coating-tool temperature that is actually measured for the TiN-YAG tool against the chip-tool temperature from the uncoated tool should introduce negligible error.

5 Discussion

The results from the experiments and the modeling involving the use of TiN-YAG tools to cut Ti6Al4V are very promising. As observed from Figure 5 and Table 1 the application of a 100-nm thick TiN coating causes a significant reduction in cutting and thrust forces, which implies that the normal and friction forces acting on the rake face are also smaller. The cutting force reduction implies that the cutting power is reduced. It is found that the total power reduces about 6.6%, whereas the friction power (found by resolving the total power into shear power and friction power, following Merchant) reduces about 28.6%. The friction power reduces much more than the total power, which is consistent with a reduction in friction coefficient at the chip-tool interface. This reduction in friction coefficient, from ~0.4 to ~0.3 is directly observable from Table 1. The reduced mechanical energy input (total and friction) should lead to a reduction in tool temperature, as suggested in Figure 4B. However, the accuracy of the temperature estimate was affected by the coating peeling problem. Attempts to keep the coating from peeling will certainly increase the accuracy of the temperature estimate, and are thus highly desirable.

While the chip-coating temperature was not measured directly, making the coating thickness small (i.e., as applied here, ~100 nm) should result in negligible difference between the chip-coating interface temperature and the coating-tool interface temperature. Therefore, comparing the coating-YAG interface temperature that was actually obtained for the TiN-YAG tool against the chip-YAG interface temperature for the uncoated tool is acceptable. This should be true even for coatings that are much thicker than the one actually applied (up to ~1 μm). Given the above, and since tool wear for the machining conditions of interest is limited to < 0.5 μm, coatings about 1 μm thick should provide both negligible temperature difference across the coating and good wear resistance. Negligible temperature difference across the coating thickness and a continuous coating layer should lead to less ambiguity in interpreting the chip-coating temperature measurements.

There is a large amount of literature (e.g., Chen, Wang, Yu, Chen, & Lu, 2014; Fei, Ling, Bo, Qing, Xun, & Rong, 2007; Yustea, Escobar-Galindoa, Carvalho, Albellaa, & Sánchez, 2011) on the emissivity of TiN, since it is actively being researched as a low-cost coating for low emissivity glass used for windows. However, the goal of this research is to achieve high transmission in the visible spectrum and high reflectivity in the mid to far infrared, so the data reported in most of the literature is not directly applicable to the TiN utilized herein. However, what is clear from this literature is that the optical and electronic properties of TiN coatings are highly dependent on coating conditions (such as the partial pressure of N_2 in chemical vapor deposition (CVD) coatings, annealing conditions that affect the crystallinity, etc.), and vary over a wide range. One exception we have found is the work of Chen et al. (Chen, Wang, Yu, Chen, & Lu, 2014), where TiN has been deposited under conditions very similar to those used at the CNST (NIST) to produce the cutting tool coatings. Chen et al. also utilized a multi-target magnetron sputtering system with a TiN target to create a TiN sample of thickness 98 nm in a pure argon atmosphere at flow rate of 30 sccm, and pressure of 0.117 Pa. For the TiN utilized herein, the argon flow rate was 50 sccm and the pressure was 0.47 Pa. Chen et al. have characterized the optical properties of the coating extensively using a spectrometer equipped with an integration sphere to measure the reflectivity. At the effective wavelength of our thermography system (~700 nm), they report a transmissivity of about 1% and a reflectivity of 50%. This reflectivity is lower than the value we find of 75%. While the reason for the increased reflectivity could be the high angle of incidence of the rays on the flank face that are reflected towards the camera, it could also be the high smoothness of the TiN-YAG interface since smoother surfaces have a higher reflectivity. Chen et al. have not reported the surface roughness of their coatings, but the free surface of the coating is usually rougher than the substrate side.

The emissivity estimation of the tool coating can be improved if the direct and reflected images can be interchanged, by cutting such that what is now the flank face is the rake face and *vice versa*. In this case the emission will be at very high angle and the reflection will be close to the normal. The

reflectivity found in such an experiment would be used to infer the emissivity for the current experiment and *vice versa*.

6 Conclusions

Addition of a 100-nm thick TiN coating that partially survives the cutting reduces friction coefficient and friction power significantly. The less severe friction causes a decrease in total power, albeit to a smaller extent. The data suggest that the tool rake face temperature also decreased, although the accuracy of the temperature measurement was affected by the lack of coating integrity throughout the cutting.

For coatings that are < 1 μm thick, the temperature difference across the coating should be close to the resolution of the imaging system (i.e., ~10 K). Based upon the finding that crater wear is no more than 0.5 μm deep, coatings that are > 0.5 μm thick should remain intact. Intact coatings should lead to less ambiguity in result interpretation. Future work will focus on the use of relatively thick coatings.

Acknowledgements

The authors would like to thank Matthew Robinson, Gerard Henein, Jessie Zhang, and Alkan Donmez of the National Institute of Standards and Technology for providing the TiN coatings as well as their characteristics reported here. This portion of the research was performed at the NIST Center for Nanoscale Science and Technology.

References

Boothroyd, G. (1963). Temperatures in Orthogonal Metal Cutting. *Proceedings of the Institution of Mechanical Engineers, 177*(29), 789-810.

Cai, S. L., & Dai, L. H. (2014). Suppression of repeated adiabatic shear banding by dynamic large strain extrusion machining. *Journal of the Mechanics and Physics of Solids, 73*, 84-102.

Carlisle, D. (2010, April). *graphicx: Enhanced support for graphics.* Retrieved from http://www.ctan.org/tex-archive/ help/Catalogue/entries/graphicx.html

Chen, F., Wang, S. W., Yu, L., Chen, X., & Lu, W. (2014). Control of optical properties of TiNxOy films and application for high performance solar selective absorbing coatings. *Optical Materials Express*, *4(9)*, 1833-1847.

Davies, M. A., Yoon, H., Schmitz, T. L., Burns, T. J., & Kennedy, M. D. (2003). Calibrated Thermal Microscopy of the Tool-Chip Interface in Machining. *Machining Science and Technology, 7*(2), 167-190. doi:10.1081/MST-120022776

Fei, Z. P., Ling, Z. G., Bo, Z. T., Qing, W. L., Xun, W. J., & Rong, H. G. (2007). Study of titanium nitride for low-e coating application. *Chinese Science Bulletin*, *52(13)*, 1860-1863.

Greene, G. A., Finfrock, C. C., & Irvine Jr, T. F. (2000). Total hemispherical emissivity of oxidized Inconel 718 in the temperature range 300-1000°C. *Experimental Thermal and Fluid Science, 22*, 145-153.

Herbert, E. (1926). The Measurement of Cutting Temperatures. *Proceedings of the Institution of Mechanical Engineers, 110*, 289-329.

Incropera, F. P., Dewitt, D. P., Bergman, T. L., & Lavine, A. S. (n.d.). *Fundamentals of Heat and Mass Transfer* (Vol. Sixth Edition). John Wiley & Sons.

Jaspers, S., Dautzenberg, J., & Taminiau, D. (1998). Temperature Measurement in Orthogonal Metal Cutting. *The International Journal of Advance Manufacturing Technology, 14*, 7-12.

Kitagawa, T., Kubo, A., & Maekawa, K. (1997). Temperature and Wear of cutting tools in high-speed machining of Inconel 718 and Ti-6Al-6V-2Sn. *Wear, 202*, 142-148.

Komanduri, R., & Hou, Z. B. (2001). A review of the experimental technique for the measurement of heat and temperatures generated in some manufacturing processes and tribology. *Tribology International, 34*, 653-682.

Kus, A., Isik, Y., Cemal Cakir, M., Coskun, S., & Özdemir, K. (2015). Thermocouple and Infrared Sensor-Based Measurement of Temperature Distribution in Metal Cuttin. *Sensors, 15*, 1274-1291. doi:10.3390/s150101274

Lane, B., Whitenton, E., Madhavan, V., & Donmez, A. (2013). Uncertainty of Temperature Measurements by Infrared Thermography for Metal Cutting Applications. *Metrologia, 50*(6), 637-653.

Marquardt, H., Speziale, S., Jahn, S., Ganschow, S., & Schilling, F. (2009). Single-crystal elastic properties of (Y,Yb)3Al5O12. *Journal of Applied Physics, 106*(093519). doi:10.1063/1.3245285

Menon, T. (2013). *Full-field infrared thermography at tool-chip interface through transparent cutting tool while machining TI-6AL-4V.* Wichita State University. Wichita State University.

Menon, T., & Madhavan, V. (2014). Infrared Thermography of the Chip-Tool Interface through Transparent Cutting Tools. *Proceedings of NAMRI/SME, 42*.

Miller, M. R., Mulholland, G., & Anderson, C. (2003). Experimental Cutting Tool Temperature Distributions. *Journal of Manufacturing Science and Engineering, 125*, 667673. doi:10.1115/1.1621425

Morikawa, J., Leong, C., Hashimoto, T., Ogawa, T., Urata, Y., Wada, S., . . . Takahashi, J.-i. (2008). Thermal conductivity/diffusivity of Nd 3 + doped Gd V O 4, Y V O 4, Lu V O 4, and Y 3 Al 5 O 12 by temperature wave analysis. *Journal of Apllied Physics, 103*(063522). doi:10.1063/1.2899181

Müller-Hummel, P., & Lahres, M. (1994). Infrared temperature measurement on diamond coated tools during machining. *Diamond and Related Materials, 3*(4-6), 765-769.

Müller-Hummel, P., & Lahres, M. (1995). Quantitative measurement of temperatures on diamond-coated tools during machining. *Diamond and Related Materials, 4*, 1216-1221.

Müller-Hummel, P., Lahres, M., Mehlhose, J., & Lang, G. (1997). Measurement of temperature on diamond-coated tools during machining processes. *Diamond Films and Technology, 7*(4), 219-232.

Narayanan, V., Krishnamurthy, K., Chandrasekar, S., Farris, T. N., & Madhavan, V. (2001). Measurement of the Temperature Field at the Tool-Chip Interface in Machining. *Proceedings of 2001 ASME International Mechanical Engineering Congress and Exposition.* New York, NY.

Pierson, H. O. (1996). *Handbook of refractory carbides and nitrides.* Noyes Publications.

Raj, V. C., & Prabhu, S. V. (2013). Measurement of surface temperature and emissivity of different materials by two-colour pyrometry. *Review of Scientific Instruments, 84*(12), 124903.

Shore, H. (1925). Thermoelectric measurement of cutting tool temperatures. *Journal of the Washington Academy of Sciences, 15*(5), 85-88.

Smart, E. F., & Trent, E. M. (1975). Temperature distribution in tools used for cutting iron, titanium and nickel. *INT. J. PROD. RES., 13*(3), 265-290.

Sutter, G., & Ranc, N. (2007). Temperature fields in a chip during high-speed orthogonal cutting - An experimental investigation. *International Journal of Machine Tools & Manufacture, 47*, 1507-1517.

Voronkov, A. (2004). *EasyChair conference system*. Retrieved from easychair.org

Wright, P. K., & Trent, E. M. (1974). Metallurgical appraisal of wear mechanisms and processes on high-speed-steel cutting tools. *Metals Technology*, 13-23.

Yustea, M., Escobar-Galindoa, R., Carvalho, S., Albellaa, J.M., & Sánchez, O. (2011). Improving the visible transmittance of low-e titanium nitride based coatings for solar thermal applications. *Applied Surface Science*, *258*, 1784–1788.